IMPROVED PERFORMANCE OF MOTOR-DRIVE SYSTEMS BY SAW SHAFT TORQUE FEEDBACK

N. Schofield[1], T. O'Sullivan[2], C. M. Bingham[2] and A. Lonsdale[3]

[1]Department of Electrical Engineering and Electronics, UMIST, Sackville Street, Manchester, M60 1QD, UK, Tel.: +44 (0)161 200 4793 Fax: +44 (0)161 200 4774
[2]Department of Electronic and Electrical Engineering, Univeristy of Sheffield, Sheffield, S1 3JD, UK
[3]Sensor Technology Limited, Balscott Mill, Balscote, Banbury, Oxon, OX15 6JB, UK
e-mail: nigel.schofield@umist.ac.uk

Abstract— The paper describes the application of a non-contact, high bandwidth, low cost, SAW-based torque measuring system for improving the dynamic performance of industrial process motor-drive systems. Background to the SAW technology and its motor integration is discussed and a resonance ratio control (RRC) technique for the coordinated motion control of multi-inertia mechanical systems, based on the measurement of shaft torque via a SAW-based torque sensor is proposed. Furthermore, a new controller structure, RRC plus disturbance feedback is proposed, which enables the controller to be designed to independently satisfy tracking and regulation performance. A tuning method for the RRC structure is given based on the ITAE index, normalized as a function of the mechanical parameters enabling a direct performance comparison between a basic proportional and integral (PI) controller. The use of a reduced-order state observer is presented to provide a dynamic estimate of the load-side disturbance torque for a multi-inertia mechanical system, with an appraisal of the composite closed-loop dynamics. The control structures are experimentally validated and demonstrate significant improvement in dynamic tracking performance, whilst additionally rejecting periodic load side disturbances, a feature previously unrealisable except by other, high-gain control schemes that impose small stability margins.

I. INTRODUCTION

With servo drive systems continually improving in performance capability, improved control of the electromechanical system dynamics is becoming an increasingly common industrial requirement. However, impulsive transient demands from such systems can excite mechanical torsional resonances in the associated drive-train, ultimately leading to controller instability, as illustrated in Fig. 1 showing tortional oscillation in a rotating shaft after the application of a 7Nm step load change, as measured via an inline instrument SAW transducer.

Practical mechanical drive systems can be complex, incorporating several non-stiff interconnecting shafts and elastic couplings, the dominant fundamental resonant frequency of which is typically <300Hz, which often overlaps with the closed-loop dynamic bandwidth imposed by the control scheme. The higher resonant modes often remain relatively unexcited, allowing a large proportion of typical industrial drive systems to be accurately modelled using a two-inertia approximation.

Until recently, difficulties in acquiring reliable, low-noise, low-cost, shaft torque transducers that are non-invasive to the mechanical drive system, have precluded the use of direct torque feedback in all but a minority of specialised closed-loop servo-drive systems. Often, commonly employed torque transducers viz. strain gauge, optical and inductive devices, are too mechanically compliant when incorporated in a drive system, thereby degrading stability margins and reducing closed-loop bandwidth. Moreover, the additional cost associated with their integration is prohibitive.

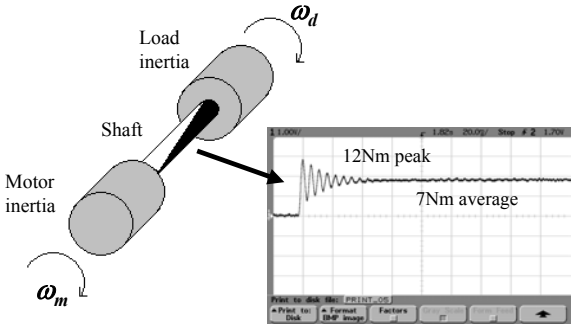

Figure 1. Measured shaft tortional oscillation immediately after the application of a 7Nm step load change.

Here then, an investigation in applying a new, low-cost, non-contact torque measurement device, based on surface acoustic wave (SAW) technology [1], is reported for use in high performance brushless machine-based servo applications, as illustrated in Fig. 2 showing a concept schematic of an servo-motor and integrated SAW sensor (a), and a commercial, brushless permanent magnet motor with integrated SAW shaft-torque feedback sensor and monitoring electronics (b).

It will be shown that direct measurement of shaft torque, coupled with a resonance ratio control strategy [2-4], can significantly enhance servo-drive system dynamics. Additionally, the use of observers is presented to directly incorporate shaft-torque feedback to provide load-side torque disturbance rejection, and the ability to design controllers for independently satisfying closed-loop tracking, and regulation performance. Conventionally the closed-loop dynamics induced by the presence of a state observer is often ignored since the observer is usually designed to be

much faster than the system dynamics. However in practice, a fast observer may lead to the undesirable amplification of high frequency noise particularly if the feedback sensors are noisy (such a the speed output from a quantized encoder). This paper therefore, provides a tuning methodology that considers the additional dynamics induced by the observer thus enabling a further reduction in observer speed.

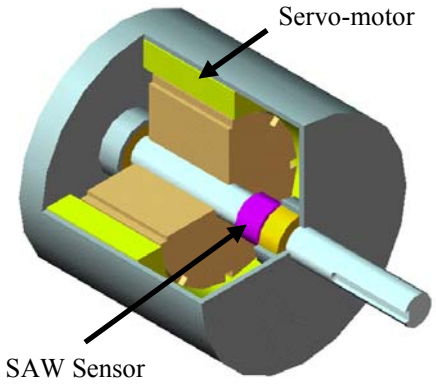

(a) Motor-sensor integration concept

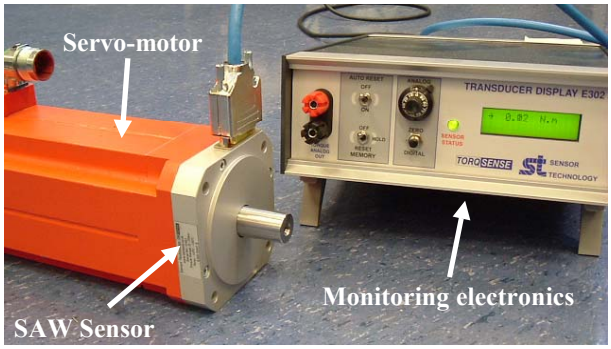

(b) Servo-motor system

Figure 2. Servo-motor, integrated SAW shaft-torque feedback sensor and monitoring electronics.

Moreover, since the SAW torque transducer exhibits a high sensitivity and bandwidth, and is largely unaffected by electromagnetic noise, it can be directly integrated into an electrical machine assembly without affecting the mechanical stiffness of the system.

II. SAW TORQUE SENSORS

Torque sensors play an important role in automatic controllers for a great variety of complex mechanical systems, from electric drills to submarines. Currently, one of the major consumers of torque sensors is the automotive industry [5]. Sensors are needed to measure torque on driveshafts and crankshafts of engines in order to optimise transmission and engine operation and improve vehicle stability. Torque sensors are also required for electrical power assisted steering systems (EPAS) that will be installed even in small cars. The benefits of automotive developments, i.e. high volume and low cost, has opened up the motor control market for SAW-based sensing systems, in-particular for motor torque feedback where significant system performance enhancements can be realised by the feedback of dynamic shaft torque information, as will be discussed latter.

Most conventional torque sensors employ a weak link (e.g. a torsion bar) to translate torque into a relatively large mechanical movement that can be measured by a potentiometer, capacitive, inductive, magnetic or optical angular position sensor. Alternatively a strain produced by the torque on the surface of the torsion bar can be measured using piezoresistive or piezoelectric strain gauges. In any case, because of the big difference between nominal measured torque (10 to 20 Nm for EPAS) and specified overload capability (10 to 30 times the nominal torque) a mechanical stop that complicates a mechanical design is usually required. Besides, many of the above mentioned sensors need a clock-spring wire connecting the shaft and the stationary interrogation unit. This also adds to complexity and cost of the sensor.

A search for a wireless device sensitive enough to omit the weak link and thus not requiring the mechanical stop has led to two most promising cost-effective candidates for high-volume applications. The first one is a magneto-elastic sensor the long-term stability of which still needs to be proven. The second one is a SAW sensor that has already demonstrated its high potential in wireless measurements of temperature, pressure, torque, force, humidity etc. [6] including those in automotive industry [5,7]. The sensitivity of SAW devices to strain is sufficient to perform the measurements on a shaft that is not weakened [8]. It greatly simplifies mechanical design and reduces the cost of the whole system. Besides, SAW sensors can withstand heat, dirt and mechanical vibration that represent problems for other types of sensor, (e.g. optical ones). The fact that SAW sensors work at radio frequencies makes it easier to arrange a non-contact coupling between the rotating shaft and the stationary interrogation unit. A careful design of the latter allows reduction of the influence of electromagnetic interference to an acceptable level.

Application of SAW devices to non-contact torque measurement was first suggested and patented in [9]. Since then the authors of the patent have fabricated and supplied torque sensors based on SAW resonators to a number of industrial customers [1,10]. Non-contact torque sensors based on SAW reflective delay lines were also introduced in [11,12].

A typical SAW torque transducer contains two SAW devices mounted on a shaft of known stiffness, as illustrated in Fig. 3. Each device consists of an array of thin metal electrodes deposited at fractional wavelengths apart on a polished piezoelectric substrate. An RF signal applied to the electrodes excites a surface

acoustic wave over the device that resonates at a frequency determined by the distance between the inter-digital metal electrodes. Torsion applied to the transducer creates two principle components of strain, S_{xx} and S_{yy}, Fig.3(a), subjecting one SAW device to tension and the other to compression. The strain varies the resonant frequency of the SAW devices, the outputs of which are connected to an RF coupler. After mixing and signal processing, the sum and difference frequencies provide shaft torque, temperature and axial stress compensation. The nominal SAW resonant frequency is typically 200MHz, with a 6200kHz difference signal equating to maximum strain. Since the SAW sensors operate at radio frequencies, a simple non-contact coupling between the rotational devices and stationary processing unit is readily achieved and, by careful design, the influence of electromagnetic interference can be reduced to acceptable levels. The temperature coefficient of the SAW devices is < 0.01% per °C for -10° to 50°C and < 0.15% per °C for 40° to 125°C. The bandwidth of the SAW transducer and signal processing unit is >2kHz. The mechanical overload capability is 300% full-scale deflection.

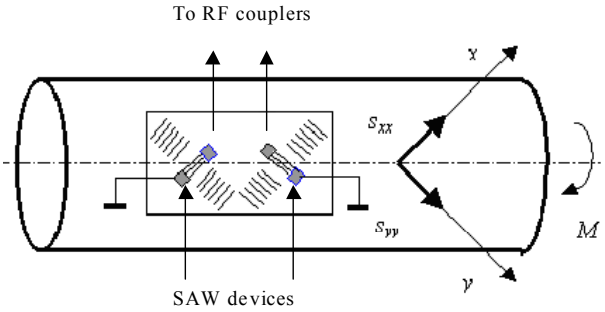

(a) Torque sensing elements based on SAW resonators

(b) SAW resonators on test shaft assembly

Figure 3. SAW-based torque transducer structure

III. MOTOR-DRIVE APPLICATION – A TWO-INERTIA MECHANICAL SYSTEM

Fig. 4(a) shows the schematic of a mechanical system containing two lumped inertias J_m and J_d representing the motor and load, respectively. The inertias are coupled via a shaft of finite stiffness K_{md}, which is subject to torsional torque t_{md}, and excited by a combination of electromagnetic torque t_e, and load torque perturbations t_d. The motor velocity is designated ω_m (rad/s) and load velocity ω_d (rad/s). Since the damping losses are generally low, they are neglected without significantly affecting the accuracy of the forgoing analysis [2-4, 13-16].

Fig. 4(b) shows a dynamic model of the two-inertia mechanical servo-drive system. The transfer functions from electromagnetic torque to motor speed, and electromagnetic torque to load speed, are described by:

$$\frac{\omega_m(s)}{t_e(s)} = \frac{s^2 + \omega_a^2}{J_m s^3 + J_m \omega_n^2 s} \quad (1) \qquad \frac{\omega_d(s)}{t_e(s)} = \frac{\omega_a^2}{J_m s^3 + J_m \omega_n^2 s} \quad (2)$$

where ω_a is the anti-resonant frequency, ω_n the resonant frequency, and R the load-motor inertia ratio:

$$\omega_a = \sqrt{K_{md}\left(\frac{1}{J_d}\right)} \quad (3) \qquad R = \frac{J_d}{J_m} \quad (4) \qquad \omega_n = \omega_a\sqrt{R+1} \quad (5)$$

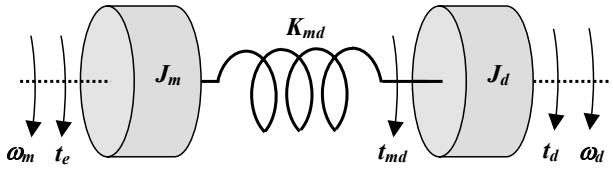

(a) Mechanical schematic

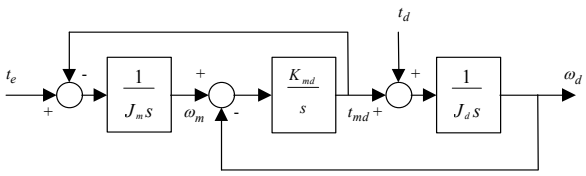

(b) Control block diagram

Figure 4. Two-inertia servo-drive system

IV. PI AND RRC CONTROL STRUCTURES

A. Tracking dynamic performance

A classical PI-type control structure is illustrated in Fig. 5(a). This control structure can be extended by augmenting a feedback signal proportional to shaft torque as illustrated in Fig. 5(b), the feedback transfer gain being K_s. Applying a feedback signal proportional to torsion in this manner is commonly referred to as Resonance Ratio Control (RRC) [2-4]. The resulting closed-loop transfer functions from reference input to load speed (tracking dynamics) for both PI and RRC structures are given in (6), with the equivalent inertia ratio, $\tilde{R}$ given in (7) for completeness.

It is noted that $\tilde{R} \rightarrow R$ as $K_s \rightarrow 0$. Tracking performance of the two control structures is evaluated using the 'integral of time multiplied by absolute error'

(ITAE) performance index for a step input, to penalise overshoot and settling time for a specified rise-time or equivalent –3dB bandwidth [17].

The step tracking dynamics of the PI-type scheme of Fig. 5(a) can be completely defined by the location of its closed-loop poles. Equating the coefficients of the characteristic equation (the denominator of (6) when K_s = 0), with the coefficients of the 4th-order ITAE polynomial (8), the system can be tuned for optimum performance, where ω_x is the equivalent –3dB bandwidth.

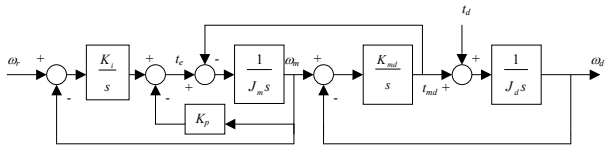

(a) PI-type controller

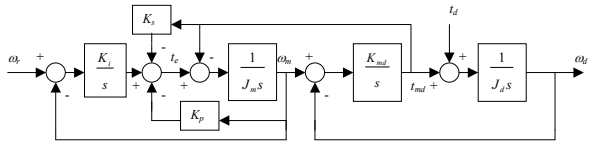

(b) RRC controller

Figure 5. Control structures for a two-inertia mechanical model of a servo-drive system

$$\frac{\omega_d}{\omega_r} = \frac{K_i \omega_a^{\,2}}{J_m s^4 + K_p s^3 + (J_m \omega_a^{\,2}(1+\tilde{R}) + K_i)s^2 + K_p \omega_a^{\,2} s + K_i \omega_a^{\,2}} \qquad (6)$$

$$\tilde{R} = R(1 + K_S) \qquad (7)$$

$$s^4 + 2.1\omega_x s^3 + 3.4\omega_x^{\,2} s^2 + 2.7\omega_x^{\,3} s + \omega_x^{\,4} \qquad (8)$$

TABLE I RRC CONTROLLER GAINS FOR OPTIMAL LOAD SIDE TRACKING PERFORMANCE

$K_S = \frac{J_m}{J_d} - 1$	$K_p \approx 1.85\omega_a J_m$	$K_i \approx 0.6\omega_a^{\,2} J_m$

Moreover, equating terms gives the optimum -3dB tracking bandwidth as $\omega_x = 0.88\omega_a$, when the motor and load inertias are matched, i.e. when R = 1. For many servo-drive system applications, where a gear reduction stage is employed, the reflected load inertia is reduced by N^2, where N is the gear reduction ratio. By analysing the closed-loop pole restrictions, the load side tracking performance of the PI controller and two-inertia system shows an increasingly underdamped response as R reduces from the optimal value, or as ω_x becomes greater than ω_a. However, by using the RRC structure when $R \neq 1$, R can be virtually adjusted to $\tilde{R}$ by the appropriate selection of K_s, thereby theoretically providing optimum performance for any R. Table I gives the optimal gains for the RRC controller.

B. Regulation dynamic performance

Equation (9) provides the closed-loop transfer function from disturbance torque to load speed (regulation dynamics), for both the PI (K_s = 0) and RRC controllers, where the inertia ratio $\tilde{R}$ for the RRC controller is expressed in (7).

From (9), it can be seen that the location of the closed-loop zeros cannot be assigned independently of the closed-loop poles, and, consequently, the closed-loop regulation and tracking dynamics cannot be independently tuned.

$$\frac{\omega_d}{t_d} = \frac{s}{J_d} \frac{J_m s^2 + K_p s + (K_i + K_{md}(1+K_s))}{J_m s^4 + K_p s^3 + (J_m \omega_a^{\,2}(1+\tilde{R}) + K_i)s^2 + K_p \omega_a^{\,2} s + K_i \omega_a^{\,2}} \qquad (9)$$

$$\frac{\omega_d}{t_d} = \frac{s}{J_d} \frac{J_m s^2 + (K_p - K_{md}K_{dd})s + (K_i + K_{md}(1+K_s - K_{pd}))}{J_m s^4 + K_p s^3 + (J_m \omega_a^{\,2}(1+\tilde{R}) + K_i)s^2 + K_p \omega_a^{\,2} s + K_i \omega_a^{\,2}} \qquad (10)$$

Here, an extended RRC control structure is introduced, as illustrated in Fig. 6(a), which includes an additional feedback signal proportional to the disturbance torque K_{pd} and its derivative K_{dd}. Equation (10) now gives the modified closed-loop transfer function describing the regulation dynamics, from where it can be seen that the closed-loop poles and zeros can be independently assigned. Assigning the closed-loop zeros to the imaginary axis (i.e. no damping of the complex conjugate zeros) for a user-defined frequency, ω_{rj}, will reject a periodic load-side disturbance of the same frequency. The required disturbance torque gains are given in (11):

$$K_{pd} = \frac{K_{md}(1+K_s) - \omega_{rj}^{\,2} J_m + K_i}{K_{md}} \qquad K_{dd} = \frac{K_p}{K_{md}} \qquad (11)$$

Periodic load-side disturbances are a common feature of industrial automated production systems, for instance, where objects are dropped at equal time intervals onto a conveyer belt. For such systems, disturbance torque cannot be sensed directly and the extended control scheme shown in Fig. 6(a) therefore requires an observer to provide a dynamic estimate. Assuming the disturbance torque is a state-variable, and its derivative is zero, a state-variable representation of the system can be obtained that includes the disturbance torque as a state (12). The measured output states can be used to reduce the complexity of the observer. In this case both ω_m and t_{md} are sensed, thereby reducing the required order of the observer to two, and therefore taking the dynamic structure shown in Fig. 6(b).

Letting $\psi = [q_1\ q_2]^t$ be an internal state vector of the observer, and $G = [g_1\ g_2]^t$ be the observer gain vector,

(13) is obtained from Gopinath's reduced order theorem [9], where X_1 and X_2 represent the measured and estimated state variables, respectively. The transfer function describing the relationship between the observed and actual load-torque can be obtained from (12) and is given by (14) where the denominator equation describes the observer pole locations. The observer poles are therefore assigned according to the coefficients of the 2nd order ITAE polynomial given in (15), where $2\varsigma_{op}$=1.414 and ω_{ob} is the equivalent –3dB observer bandwidth. The observer gains G_1 and G_2 are given by (16) and (17) respectively.

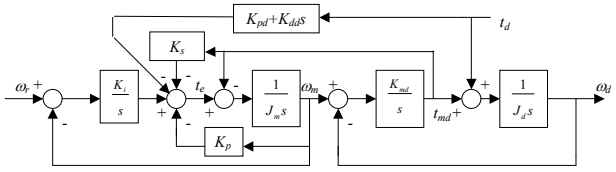

(a) RRC controller plus disturbance feedback

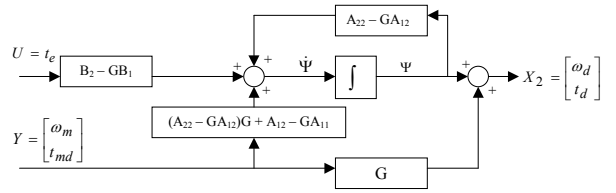

(b) Reduced order observer

Figure 6. Control structures for a two-inertia mechanical model of a servo drive system

$$\frac{d}{dt}\begin{bmatrix} \omega_m \\ t_{md} \\ \omega_d \\ t_d \end{bmatrix} = \left[\begin{array}{cc:cc} 0 & -\frac{1}{J_m} & 0 & 0 \\ K_{md} & 0 & K_{md} & 0 \\ \hdashline 0 & \frac{1}{J_d} & 0 & -\frac{1}{J_d} \\ 0 & 0 & 0 & 0 \end{array}\right] \bullet \begin{bmatrix} \omega_m \\ t_{md} \\ \omega_d \\ t_d \end{bmatrix} + \begin{bmatrix} \frac{1}{J_m} \\ 0 \\ 0 \\ 0 \end{bmatrix} t_e \qquad (12)$$

$$= \left[\begin{array}{c:c} A_{11} & A_{12} \\ \hdashline A_{21} & A_{22} \end{array}\right] \bullet \begin{bmatrix} X_1 \\ X_2 \end{bmatrix} + \begin{bmatrix} B_1 \\ B_2 \end{bmatrix} U$$

$$\dot{\psi} = X_2(A_{22} - GA_{12}) + X_1(A_{21} - GA_{11}) + (B_2 - GB_1)u \qquad (13)$$
$$\psi = X_2 - GX_1$$

$$\frac{G_2\omega_a^{\,2}}{s^2 + s(-G_1K_{md}) + G_2\omega_a^{\,2}} \qquad (14) \qquad s^2 + 2\varsigma_{ob}\omega_{ob}s + \omega_{ob}^{\,2} \qquad (15)$$

$$G_1 = \frac{-1.4\omega_{ob}}{K_{md}} \qquad (16) \qquad G_2 = \frac{\omega_{ob}^{\,2}}{\omega_a^{\,2}} \qquad (17)$$

If the observer pole locations are assigned to be much greater than the closed loop zeros in (10), it can be assumed that the observer dynamics do not unduly influence the performance of the closed-loop regulation dynamics. However, in practice the observer poles cannot be placed significantly higher since there exists a trade-off between the bandwidth of the observer and filtering of high frequency noise generated by the sensing devices and/or the power amplifier. Moreover, in the case of the proposed control scheme, where the derivative of the observed load torque is required, the attenuation of high frequency noise is of greater importance if the control scheme is to be practically realisable.

Consider Fig. 7, which is identical to the control structure of Fig. 6(a) except the observer dynamics are included in the disturbance feedback. Equation (18) now gives the modified closed-loop transfer function describing the regulation dynamics, where it can be seen that the numerator now contains two pairs of complex zeros that can be independently assigned by the selection of the observer gains G_1 and G_2, and the disturbance feedback gains K_{pd} and K_{dd}. Thus, by proper adjustment of these gains, the closed-loop system dynamics can be tuned to reject a specific user defined frequency whilst eliminating the effects of the observer dynamics on the rejection performance, i.e. a relatively slow disturbance observer can be implemented, attenuating high frequency noise, without sacrificing the control objective.

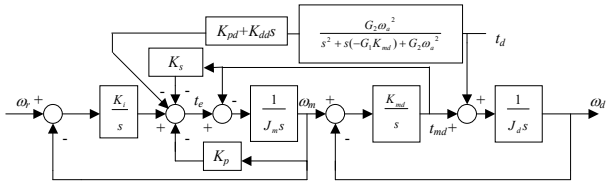

Figure 7. RRC controller plus observer disturbance feedback

$$\frac{\omega_d}{t_d} = \frac{s}{J_d} \frac{\left\{\begin{array}{l} J_m s^4 + (K_p - G_3K_{md}J_m)s^3 \\ + (G_4\omega_a^{\,2}J_m - G_3K_{md}K_p + [K_i + K_{md}(1+K_s)])s^2 \\ + (G_4\omega_a^{\,2}K_p - G_3K_{md}[K_i + K_{md}(1+K_s)] - J_dK_{dd}G_4\omega_a^{\,2})s \\ + G_4\omega_a^{\,2}[K_i + K_{md}(1+K_s)] - J_dK_{pd}G_4\omega_a^{\,4} \end{array}\right\}}{\left\{\begin{array}{l} (J_m s^4 + K_p s^3 + (J_m\omega_a^{\,2}(1+\tilde{R}) + K_i)s^2 + K_p\omega_a^{\,2}s + K_i\omega_a^{\,2}) \\ \cdot (s^2 - G_3K_{md}s + G_4\omega_a^{\,2}) \end{array}\right\}} \qquad (18)$$

$$(s^2 + \omega_{rj}^{\,2})(s^2 + 2\varsigma_2\omega_2 + \omega_2^{\,2}) \qquad (19)$$

Equation (19) shows a general expression describing two pairs of complex zeros, where the first root represents the user defined rejection frequency, ω_{rj} (damping equals zero), and the other root defines the arbitrary location of the second pair of complex zeros. By comparing the numerator of (18) with (19), expressions can be derived that enable ω_{rj} and the observer pole locations to be independently assigned as follows:

$$\varsigma_2\omega_2 = \frac{K_p + 2\varsigma_{ob}\omega_{ob}J_m}{2J_m} \qquad (20)$$

$$\omega_2 = \sqrt{\frac{\omega_{ob}^2 J_m + K_{md}(1+K_s) + K_i + 2\zeta_{ob}\omega_{ob}K_p - \omega_a^2}{J_m}} \quad (21)$$

$$K_{pd} = \frac{G_4\omega_a^2\left[K_i + K_{md}(1+K_s)\right] - \omega_{rj}^2\omega_2^2 J_m}{J_d G_4 \omega_a^4} \quad (22)$$

$$K_{dd} = \frac{G_4\omega_a^2 K_p + 2\zeta_2\omega_{rj}\omega_2 J_m - G_3 K_{md}\left[K_i + K_{md}(1+K_s)\right]}{J_d G_4 \omega_a^4} \quad (23)$$

TABLE II MECHANICAL PARAMETERS

R	0.5	J_d	0.00145 kgm^2
J_m	0.0029 kgm^2	K_{md}	110 Nm/rad
ω_a	275.43 rad/s		

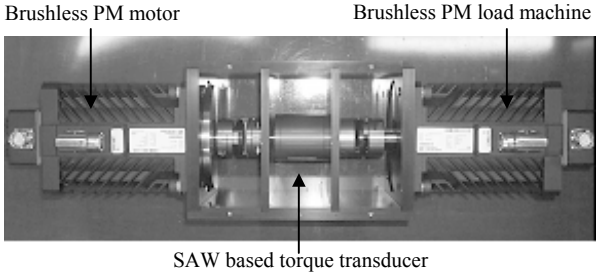

(a) Mechanical system overview

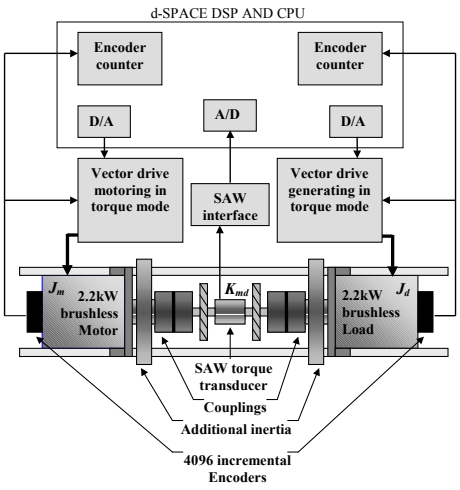

(b) Functions of components

Figure 8. Experimental facility, components and control system

V. PERFORMANCE EVALUATION

Dynamic simulation models of the proposed control structures have been implemented in Matlab/Simulink and subsequently validated on an experimental test-facility, as illustrated in Fig. 8. The test facility comprises of 2×2.2kW brushless permanent magnet (PM) servo-machines mounted in a back-to-back configuration to provide a servo-drive and dynamic load, as described by the mechanical parameters given in Table II. An integrated 20Nm, SAW-based torque transducer forms the interconnecting shaft between the two servo-machines, Fig. 8(a), and is used to realize the RRC and disturbance rejection control structures. The control algorithms, sensor inputs and control outputs are realized via a DSP-based, d-SPACE system as illustrated schematically in Fig. 8(b).

A. Tracking performance

The RRC controller gains K_p , K_i and K_s are tuned optimally according to Table I. Fig. 9 shows simulated results from the system in response to a step change in reference velocity of 10 rad/s. Fig. 9(a) shows the dynamics resulting from the PI control structure, whilst Fig. 9(b) shows the RRC-induced dynamics. It can be seen that since $R < 1$ ($R = 0.5$), the PI controller imparts an underdamped response, particularly at the load side, whilst the RRC controller 'virtually' increases R resulting in optimal load-side tracking performance.

For comparison, experimental tracking results are presented in Fig. 10, illustrating the validity of the controller scheme. Note, the extra flexibility afforded by RRC is shown to be sufficient to simultaneously impart optimal closed-loop load-side performance whilst also allowing the independent or virtual selection of inertia ratio.

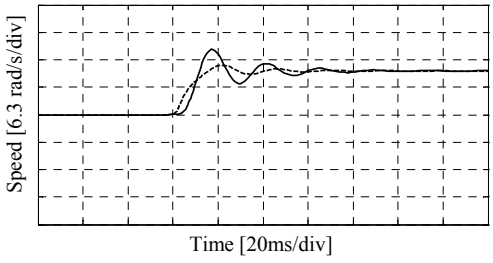

(a) PI controller with $\omega_x = 0.88\omega_a$

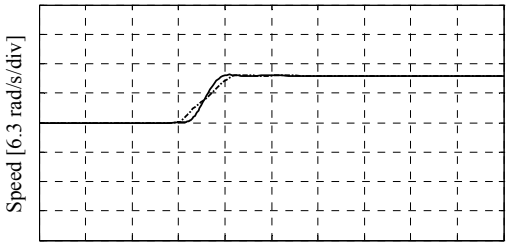

(b) RRC controller with $\omega_x = 0.88\omega_a$

Figure 6. Simulated tracking step responses for the two-inertia servo-drive system

B. Regulation performance

With identical control gains as for the tracking performance evaluation, the regulation performance is evaluated via the closed-loop systems ability to reject a sinusoidal load-side disturbance. By way of example, the load-side disturbance is a 4Nm, 62.8 rad/s (10Hz) sine wave generated by the load servo-machine of Fig. 8(a). Two case studies are considered:

Case (i) – where the disturbance torque feedback is

assumed ideal and the effects of the observer are of sufficient bandwidth that they can be neglected. The disturbance feedback gains K_{pd} and K_{dd}, are initially chosen according to (11) and (12) where ω_{rj} = 62.8 rad/s; and

Case (ii) – here a non-ideal disturbance observer is assumed. The disturbance gains are now chosen according to (20-23) where ω_{rj} = 62.8 rad/, i.e. the disturbance torque feedback is assumed non-ideal and the dynamics of the disturbance observer are included in the tuning procedure.

It was found that when disturbance feedback was implemented, a disturbance observer with a bandwidth ω_{ob} > 50Hz ($5\omega_{rj}$ in this case) caused controller instability due to the noise injected into the closed-loop system. Consequently, to provide valid experimental results, the observer bandwidth was limited to $\omega_{ob} \leq 3\omega_{rj}$.

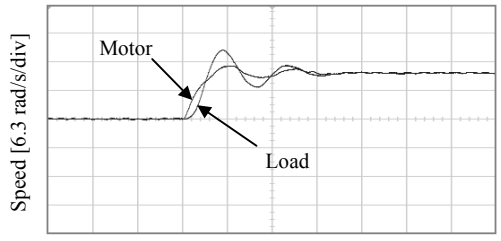

(a) PI controller with $\omega_x = 0.88\omega_a$

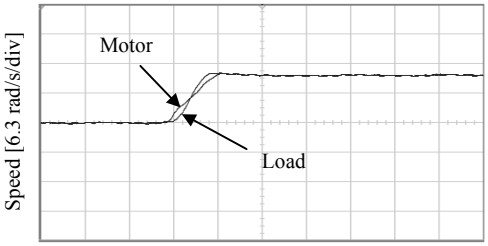

(b) RRC controller with $\omega_x = 0.88\omega_a$

Figure 10. Measured tracking step responses for the experimental two-inertia servo-drive system

Figure 11 illustrates the regulation response when no disturbance feedback is implemented within the controller structure showing both the load-speed and the shaft-torque. Fig. 12(a) illustrates the responses with disturbance feedback when the feedback gains are chosen assuming an ideal disturbance observer, case (i) and Fig. 12(b) assuming a non-ideal disturbance observer, case (ii), where for each case, $\omega_{ob} = 3\omega_{rj}$.

To illustrate the effects of a further reduction in observer speed, the experimental results in Fig. 12 are repeated for $\omega_{ob} = 1.5\omega_{rj}$, i.e. the observer bandwidth is halved, the results being presented in Figs. 13. It can be seen by comparison of Figs. 12(a) and 13(a) that reducing the speed of the observer for case (i) significantly deteriorates the control objective i.e. the attenuation of the load-torque perturbations is further reduced and comparable with the results obtained with no disturbance feedback (Fig. 11).

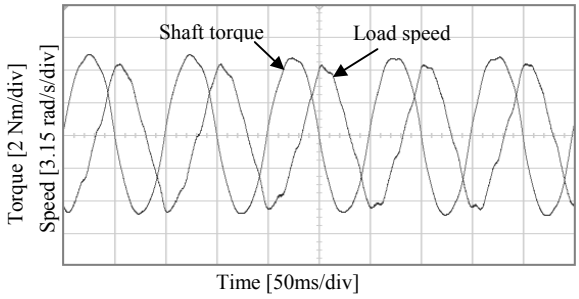

Figure 11. Experimental regulation responses with no disturbance feedback

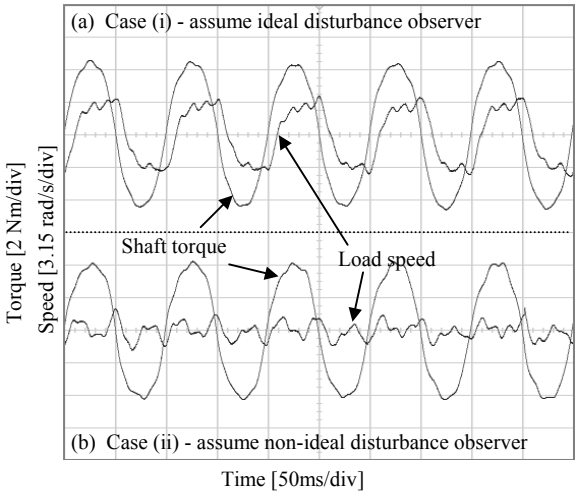

Figure 12. Experimental regulation responses with disturbance feedback; $\omega_{ob} = 3\omega_{rj}$

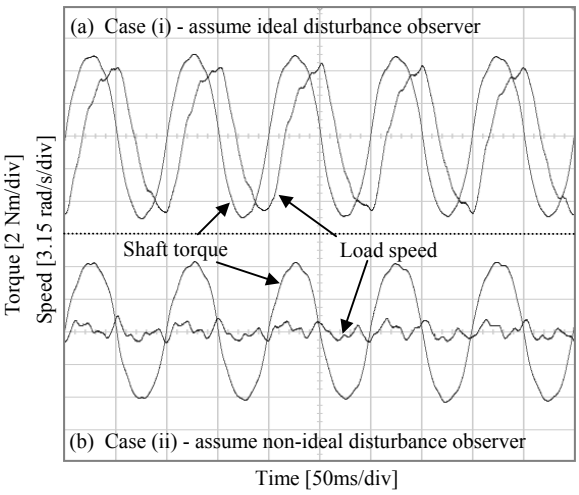

Figure 13. Experimental regulation responses with disturbance feedback; $\omega_{ob} = 1.5\omega_{rj}$

Comparing Figs. 12(b) and 13(b) for case (ii), it can be seen that the load perturbations are now rejected from the load-speed and the rejection performance is not

unduly influenced by the speed of the observer. This is of significant practical importance for the system under investigation where sensor noise (torque transducer and encoder in this case) has a significant impact on the allowable speed of the observer.

VI. CONCLUSIONS

A comparative study of compensation schemes for the control of multi-inertia mechanical systems has been reported. An improved technique based on the measurement of shaft torque using a SAW-based torque sensor is demonstrated to improve dynamic tracking performance, whilst additionally rejecting periodic load side disturbances. The proposed scheme allows assignment of the closed-loop zeros, thus enabling the rejection of a specific periodic load disturbance, and independent tuning of tracking and regulation dynamics.

Integration of the SAW sensor inside a servo-motor is viable, leading to a compact unit suitable for industrial servo-control applications.

VII. ACKNOWLEDGEMENTS

The authors acknowledge the UK Engineering and Physical Science Research Council (EPSRC), and Sensor Technology Ltd., Banbury, UK, for the provision of an EPSRC CASE studentship.

VIII. REFERENCES

[1] Lonsdale, A., "Dynamic rotary torque measurement using surface acoustic waves," *Sensors*, Vol. 18, no. 10, Oct. 2001, pp. 51-56.

[2] Hori, Y., Sawada, H. and Chun, Y., "Slow resonance ratio control for vibration suppression and disturbance rejection in torsional system," *IEEE Trans. Ind. Elect.,* Vol. 46, No. 1, February 1999, pp. 162-8.

[3] Yuki, K., Murakami, T., Ohnishi, K., "Vibration control of 2-mass resonant system by resonance ratio control," *International Conference on Industrial Electronics, Control, and Instrumentation (IECON '93)*, Vol. 3, 15-19 Nov. 1993, pp. 2009-14.

[4] Mortimoto, S., Hamamoto, A., Takeda, Y., "Vibration control of two-mass system with low inertia ratio considering practical use," *Electrical Engineering in Japan*, Vol. 125, No. 2, 1998, pp. 1-9.

[5] Jerems, F., Proft, M., Rachui, D. and Kalinin, V., "A new generation non-torsion bar torque sensors for electromechanical power steering applications", *Proc. Int. Congress on Electronic Systems for Vehicles,* Baden Baden, September, 2001, pp. 27-28.

[6] Schmidt, F., Scholl, G., "Wireless SAW identification and sensor systems", in *Advances in Surface Acoustic Wave Technology, Systems and Applications*, vol. 2, C. C. W. Ruppel and T. A. Fjeldly, Eds. Singapore: World Scientific, 2001, pp. 277-325.

[7] Pohl, A., Seifert, F., "Wirelessly interrogable surface acoustic wave sensors for vehicular applications", *IEEE Trans. Instrum. Meas.*, vol. 46, 1997, pp. 1031-1038.

[8] Gullen, D.E., Reeder, T.M. "Measurement of SAW velocity versus strain for YX and ST quartz", *Proc. Ultrason. Symp.,* 1975, pp. 519-522.

[9] Lonsdale, A., Lonsdale, B. "Method and apparatus for measuring strain", Int. patent public. No. WO 91/13832, 19 Sept. 1991, Int. Applic. No. PCT/GB91/00328, Int. filing date: 4 March 1991, Priority: 9004822.4, 3 March 1990, GB.

[10] Merewood, P., "A novel ZnO/Si thin-film SAW torque measurement microsystem", *Int. Forum on Wave Electron. and Its Applications,* St.-Petersburg, 14-18 Sept., 2000.

[11] Wolff, U., Schmidt, F., Scholl, G., Magory, V., "Radio Accessible SAW sensors for non-contact measurement of torque and temperature", *Proc. IEEE Ultrason. Symp.,* 1996, pp. 359-362.

[12] Grossmann, R., Michel, J., Sachs, T., Schrufer, E., "Measurement of mechanical quantities using quartz sensors", *Proc. Europ. Freq. Time Forum,* 5-7 March, 1996, pp. 376-381.

[13] Euteback, T., Pacas, J. M., "Damping of torsional vibrations in high-dynamic-drives," *8th European Conference on Power Electronics and Applications (EPE'99)*, CD-ROM, Brussels, Belgium, 1999, pp. 10.

[14] Menne, M., Bitsche, O., "Comparison of drivetrain oscillation damping-algorithms for electric vehicles," *Electric Vehicle Symposium (EVS 18)*, Berlin, 2001.

[15] Solbodan N.V., Stojic, M.R., "Suppression of torsional oscillations in a high performance speed servo drive," *IEEE Trans. Ind. Elect*., Vol. 45, No. 1, Feb. 1998.

[16] O'Sullivan, T.M., Schofield, N., Bingham, C.M., "Simulation and experimental validation of induction machines dynamics driving multi-inertia loads," *Journal of Applied Electromagnetics and Mechanics (JAEM)*, Vol. 19, (2003).

[17] Franklin, G., Powell, D., and Emami-Naeini, A., "Feedback Control of Dynamic Systems", *book*, Prentice-Hall, ISBN: 0-13-032393-4, 2002.